ACES Asian Chemical Editorial Society

doi.org/10.1002/cnma.202200122

CHEMNANOMAT
Research Article

www.chemnanomat.org

Methanol Tolerant Oxygen Reduction Reaction Electrocatalysis using Size-Specific Triphenylphosphine-Ligated Gold Nanoclusters

Hanieh Mousavi,[a] Shailendra K. Sharma,[b] Vladimir Golovko,[b] Cameron J. Shearer,*[a] and Gregory F. Metha*[a]

Abstract: The development of a stable and efficient Oxygen Reduction Reaction (ORR) electrocatalysts with high methanol tolerance is crucial for Direct Methanol Fuel Cells (DMFCs). Herein, triphenylphosphine (PPh_3)-ligated gold nanoclusters and complexes (AuNCs), $Au_{101}(PPh_3)_{21}Cl_5$, $Au_9(PPh_3)_8(NO_3)_3$, and $Au_1(PPh_3)Cl$ supported on reduced graphene oxide (rGO) have been explored as methanol tolerant ORR electrocatalysts. Electrocatalytic performance of each AuNCs-rGO was determined through linear sweep voltammograms (LSV) and cyclic voltammetry (CV) and compared with Pt/C. Size-dependent ORR activity was observed which followed the size trend of Au_{101}NC-rGO > Au_9NC-rGO > Au_1NC-rGO. Repeated LSV and chronoamperometry measurements revealed that the long-term stability over 24 hours followed the trend Au_{101}NC-rGO > Au_9NC-rGO ~ Au_1NC-rGO and all were more stable than Pt/C. The methanol tolerance of each AuNCs-rGO was also evaluated *via* LSV and CV. Size-independent methanol tolerance with no noticeable change in ORR performance of AuNCs-rGO was observed in the presence of methanol. AuNCs-rGO nanocomposites are promising cathode electrocatalysts for DMFCs.

1. Introduction

Direct Methanol Fuel Cells (DMFCs) generate electric power from methanol and air without the need for combustion. Methanol is a desirable fuel due to its simpler storage and distribution compared to hydrogen. In addition, it provides higher volumetric energy density (15.8 MJ/L)[1] compared to both liquid (8.4–10.4 MJ/L)[1] and compressed (5.6 MJ/L at 700 bar) hydrogen.[2] Methanol can be produced from biomasss and therefore offers a more renewable energy source than fossil fuels.[3] With further developments in CO_2 conversion, it may become possible to convert CO_2 to methanol and therefore create a recyclable energy system.[4] However, the basic operational principles in alkaline DMFCs have inherent losses at both the anode and cathode. Figure 1 presents a general scheme of DMFCs. The overall ORR efficiency at the cathode is limited by two losses. The major loss occurs from methanol diffusion across the membrane from the anode compartment to the cathode. Typical ORR electrocatalysts at the cathode have low tolerance towards methanol, especially at high methanol concentration, and consequently the catalyst is poisoned which results in a loss of cell efficiency (approximately 0.1 V at the oxygen electrode).[5,6] The second source of loss is the large overpotential required to drive O_2 reduction (ORR, about 0.2 V) which results in 20% loss from the theoretical efficiency.[5]

Platinum (Pt) has been broadly studied as a crucial metal in electrocatalysts used in DMFCs to improve ORR.[7] However, after methanol cross over, methanol competes with O_2 for the active sites on the Pt surface leading to a mixed potential caused by the simultaneous occurrence of the methanol oxidation reaction (MOR) and ORR at the cathode. Furthermore, partial oxidation of the adsorbed methanol produces CO, which binds strongly to the Pt surface leading to poisoning of the active sites on Pt and results in greater loss of cell efficiency.[8] Therefore, the ORR electrocatalysts in DMFCs must be methanol tolerant.

Compared to Pt, bulk gold (Au) has attracted less research interest in catalysis such as ORR and MOR. Density functional theory (DFT) has predicted that Au is less active than Pt for ORR due to a larger O=O dissociation energy.[9] Additionally, the onset potential of Au for MOR in both direct and indirect mechanisms (Figure 1) is also higher than Pt due to the larger ΔG_{CO} (Gibbs free energy for CO formation) for Au than Pt.[10] These DFT findings suggest that, although bulk Au has a high overpotential for ORR, it also has a high overpotential for MOR which opens the possibility of methanol tolerant electrocatalysts if the ORR activity can be improved.

In recent decades, sub-2 nm sized gold nanoclusters and complexes (AuNCs) have been explored as promising electrocatalysts for ORR,[11–24] hydrogen evolution reaction (HER),[25] hydrogenation of terminal alkynes into alkenes,[26] CO oxidation,[27] styrene oxidation[28,29] and benzyl alcohol oxidation.[30,31]

The unusual catalytic behaviour of the AuNCs compared to bulk Au is due to a series of size-dependant properties,

[a] H. Mousavi, Dr. C. J. Shearer, Prof. G. F. Metha
Department of Chemistry, University of Adelaide, Adelaide SA 5005, Australia
E-mail: cameron.shearer@adelaide.edu.au
greg.metha@adelaide.edu.au

[b] Dr. S. K. Sharma, Assoc. Prof. V. Golovko
The MacDiarmid Institute for Advanced Materials and Nanotechnology, School of Physical and Chemical Sciences, University of Canterbury, Christchurch 8140, New Zealand

Supporting information for this article is available on the WWW under https://doi.org/10.1002/cnma.202200122

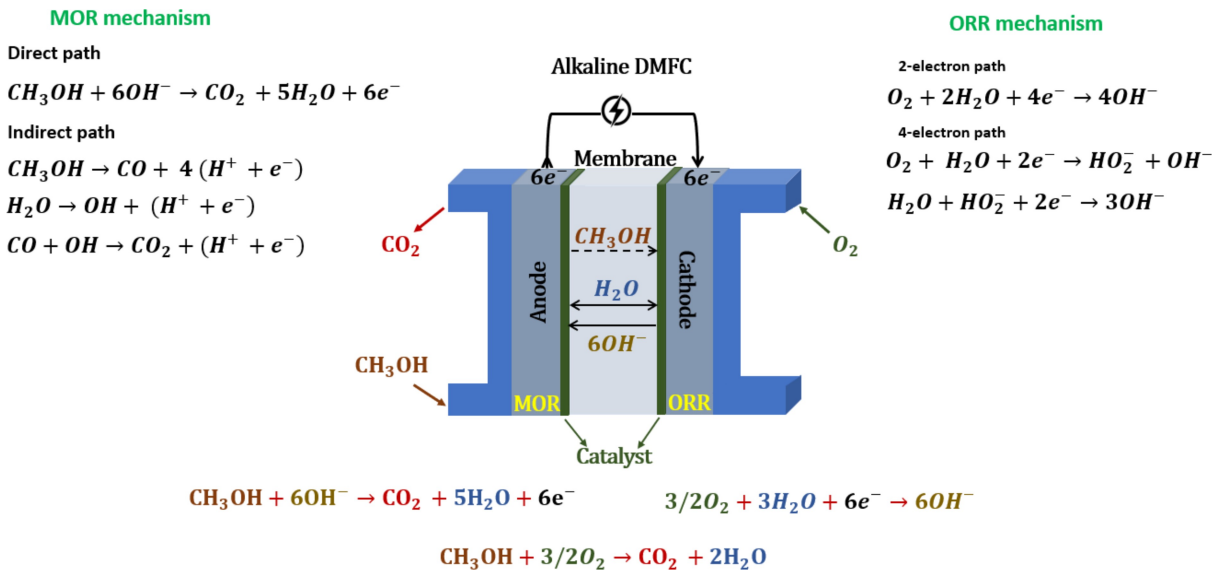

Figure 1. Schematic of an alkaline direct methanol fuel cell (DMFC) showing the methanol oxidation reaction (MOR) at the anode and oxygen reduction reaction (ORR) at the cathode.

including high surface-to-volume ratio,[15,32,33] molecular-like electronic properties,[34] and ligand density (if present).[15] In addition, the type of ligand[15] and immobilization of AuNCs onto a support[13] provide an effective method to increase or tailor the catalytic activity of AuNCs.

Table S1 summarises the key parameters of previous studies investigating ORR activity and methanol tolerance of AuNCs. Decreasing AuNCs cluster size not only increases the number of Au atoms on the surface but also alters the electronic properties. Theoretical and experimental research has determined that by decreasing the cluster size, the 5d-electron density increases and shifts the d-band toward the Fermi level, which is favourable for oxygen adsorption.[35,36] Amongst the literature (Table S1), the trend of reduced AuNCs size leading to greater ORR electrocatalytic activity has been reported for a number of AuNCs.[11,15,16,19] Interestingly, not all reports show that smaller AuNCs size results in greater activity which can be explained by the role of ligands.[17,18]

The role of the ligand is complex; although it is required to maintain the cluster size, it also has an effect on catalytic performance. The ligand can alter the electronic properties of the AuNCs and also sterically hinder analyte diffusion and adsorption to the surface. Despite the fact that ligand removal is considered as a pathway to make more available active sites, it is challenging to retain the cluster size without ligands.[16–24] AuNCs ligands are typically organo-thiols or phosphines but can have a wide variety of organic functionality, which can alter the reactivity of AuNCs.[37] For instance, AuNCs protected by bulky ligands have lower ligand density, particularly at larger sizes, resulting in higher ORR activity compared to aliphatic and linear ligands.[17] Additionally, aliphatic and linear ligands with the long chain lengths result in larger distances between the Au core and electrode leading to lower electron transfer and ORR activity.[15] Current AuNCs synthesis methods cannot alter cluster size without changing the ligand density, typically the larger AuNCs having lower ligand density, and therefore their effect cannot be decoupled.

The combination of ligand type, ligand density and AuNCs size explains the two contrasting trends observed for ORR activity with AuNCs size (Table S1). The AuNCs with linear ligands[15,16] are less affected by ligand density and consequently their ORR activity increases with decreasing size due to the different electronic properties of the smaller AuNCs. In contrast, AuNCs with bulky ligands[17,18] are significantly affected by their ligands which results in greater ORR activity with increasing size due to the lower ligand density of larger AuNCs.

Recent studies have shown that reduced graphene oxide (rGO) as a support can improve the efficiency of both redox reactions in fuel cells[13,14,20–22,38] due to its unique properties, including high electrical conductivity, large surface area, and high charge mobility.[39] In addition, aggregation of AuNCs is prevented due to the strong metal support interaction between rGO and metal clusters.[25] DFT calculations have suggested that hybridization of Au with graphene materials can result in a highly active and stable ORR electrocatalyst.[40,41] Therefore, there is an emerging interest to develop AuNCs-based nanocomposites using graphene-related materials.

Herein, the ORR activity and methanol tolerance of $Au_{101}(PPh_3)_{21}Cl_5$ and $Au_9(PPh_3)_8(NO_3)$ nanoclusters and the $Au_1(PPh_3)Cl$ complex supported on rGO are explored, compared and assessed for the first time.

2. Results And Discussion

2.1. Experimental Results

2.1.1. AuNCs-rGO synthesis

Two of our previous publications were dedicated to the formation of AuNCs-rGO nanocomposites without AuNCs agglomeration.[25,42] The AuNCs-rGO were synthesised *via* mixing a methanol dispersion of AuNCs and rGO for 1 h at RT in the dark. We discovered that the GO reduction method under acidic pH (pH≈2) is crucial to avoid the agglomeration of AuNCs. Figure S1 shows HAADF-STEM images for the as-prepared AuNCs-rGO indicating the deposition of AuNCs on rGO without agglomeration. Complete characterisation of the AuNCs and AuNCs-rGO are described in our previous publications.[25,42] Of particular note, we confirmed a gold mass loading of 4.7% (Au_1NC-rGO), 4.3% (Au_9NC-rGO), and 4.8% (Au_{101}NC-rGO) through a combination of thermogravimetric analysis and inductively coupled plasma mass spectrometry.

2.1.2. Oxygen Reduction Reaction activity investigation of AuNCs-rGO

The ORR electrocatalytic activity of Au_1NC-rGO, Au_9NC-rGO, and Au_{101}NC-rGO along with rGO, Au_1, Au_9, Au_{101}, bare GCE (glassy carbon electrode), and Pt/C were evaluated using cyclic voltammetry (CV) and linear sweep voltammetry (LSV) in alkaline media on a static GCE. Firstly, the electrochemical activity of all samples toward ORR was characterized by CV in N_2 and O_2-saturated 0.1 M KOH (Figure 2 and Figure S6). An explicit characteristic cathodic ORR polarization curve is clearly observed in the O_2-saturated electrolyte in contrast to the featureless CV in the N_2-saturated electrolyte for all samples.

LSV ORR polarization curves for Au_1NC-rGO, Au_9NC-rGO, Au_{101}NC-rGO, rGO, bare GCE, and Pt/C (Figure 3a) along with Au_1, Au_9, Au_{101}, and bare GCE (Figure S7) in O_2-saturated 0.1 M KOH solution were also performed. Similar to the CV results, the LSV curves present a well-defined ORR response for all samples. Au_1NC-rGO, Au_9NC-rGO, and Au_{101}NC-rGO are shifted positively (lower overpotential) compared to the bare GCE, rGO, and unsupported AuNCs. Additionally, the ORR activity improves from Au_1NC-rGO < Au_9NC-rGO < Au_{101}NC-rGO. The ORR activity of Au_1NC-rGO, Au_9NC-rGO, and Au_{101}NC-rGO is quantitatively evaluated (details in Figure S5) with the three parameters; onset potential, half-wave potential ($E_{1/2}$), and current density at 0.8 V *vs.* RHE (Table 1).

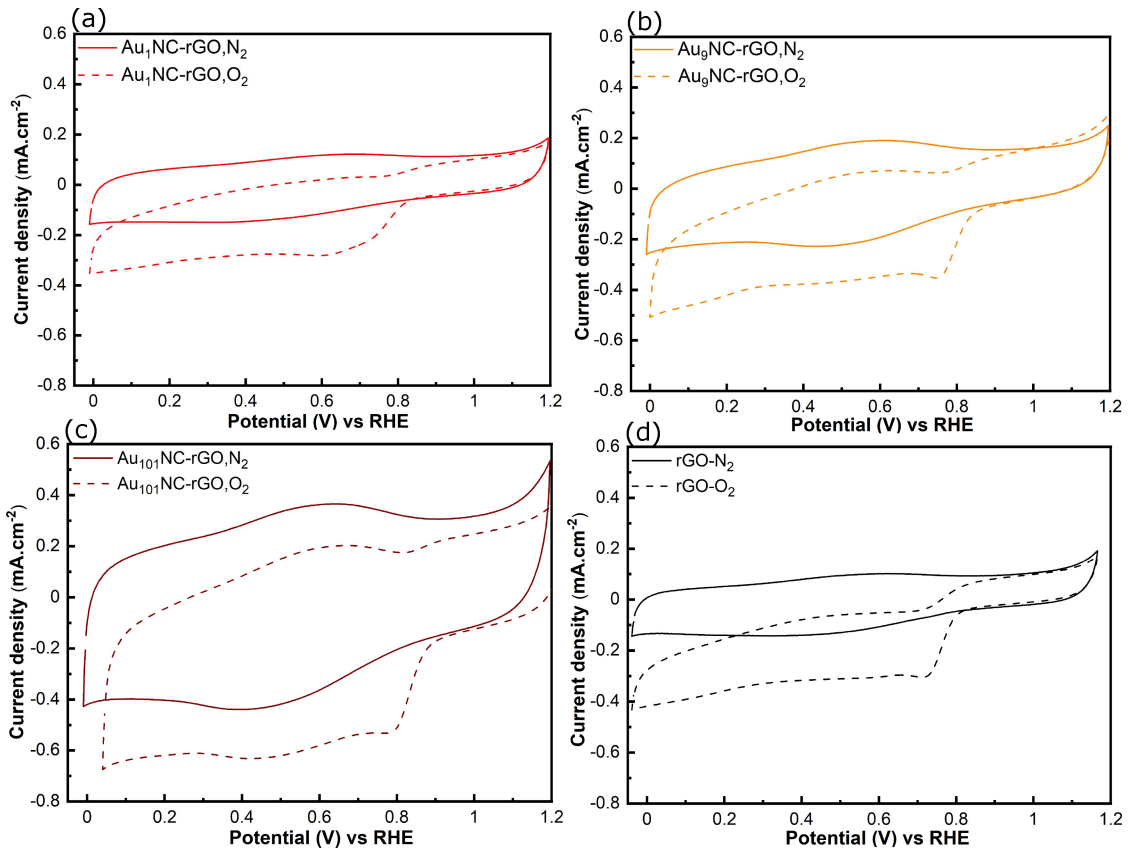

Figure 2. (a–d) CV curves of Au_1NC-rGO, Au_9NC-rGO, Au_{101}NC-rGO, and rGO at a scan rate of 10 mV s^{-1} in N_2 and O_2-saturated 0.1 M KOH.

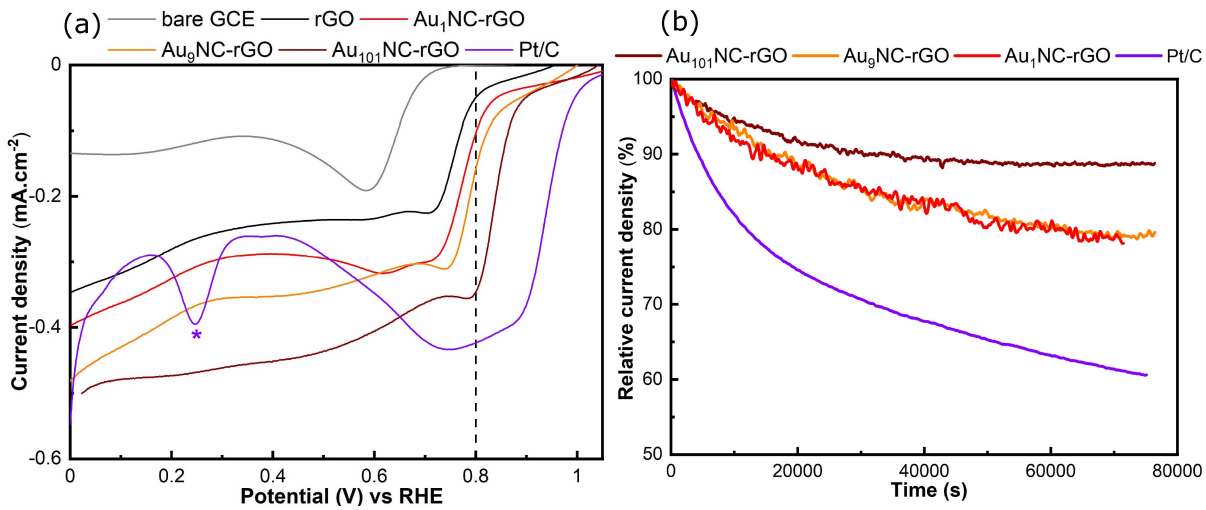

Figure 3. (a) ORR polarization curves of bare GCE, rGO, Au_1NC-rGO, Au_9NC-rGO, Au_{101}NC-rGO, and Pt/C (b) stability test at $E_{1/2}$ over 22 h for Au_1NC-rGO, Au_9NC-rGO, Au_{101}NC-rGO, and Pt/C. All data was collected at a scan rate of 10 mV s^{-1} in O_2-saturated 0.1 M KOH under continuous O_2 flow. *Hydrogen adsorption peak of Pt/C.[43]

Table 1. Summary of the ORR and electrochemical properties of the investigated AuNCs-rGO calculated with respect to geometric surface area, ECSA, and Au mass loading. E_{onset}, $E_{1/2}$, and current density at 0.8 V (vs. RHE) were determined from ORR polarization curves in O_2-saturated 0.1 M KOH. Double-layer capacitance (C_{dl}) and ECSA were determined from CV at different scan rates in N_2-saturated 0.1 M KOH.

Catalyst	E_{onset} (V)	$E_{1/2}$ (V)	Current Density at 0.8 V (*vs.* RHE) mA cm_{geo}^{-2}	mA $ECSA^{-1}$	mA mg_{Au}^{-1}	C_{dl} (μF cm^{-2})	ECSA (cm^2)
Au_1NC-rGO	0.87 ± 0.006	0.77 ± 0.007	−0.10	−0.15	−40.8	0.020	0.048
Au_9NC-rGO	0.87 ± 0.007	0.79 ± 0.010	−0.16	−0.23	−62.5	0.021	0.050
Au_{101}NC-rGO	0.93 ± 0.010	0.84 ± 0.008	−0.35	−0.45	−136.3	0.023	0.056

As the actual surface area of a catalyst is affected by different parameters such as porosity, defects and morphological structure, there might be a difference between electrochemical active surface area (ECSA) and geometric area. Therefore, the electrocatalytic activity of AuNCs per geometric area, ECSA, and also Au mass was assessed. The mass of Au was the same for each AuNCs (0.16 μg = 2.25 μg cm^{-2} non-ligated Au mass). The ECSA was determined *via* CV (details in Figure S9) for each electrocatalyst to be 0.048, 0.050, 0.056 cm^2 for Au_1NC-rGO, Au_9NC-rGO, and Au_{101}NC-rGO, respectively. The ORR polarization curves per Au mass and ECSA are plotted in Figure S10 (a–b), and the current density (at 0.8 V *vs.* RHE) from these plots is presented in Table 1 (mA $ECSA^{-1}$ and mA mg_{Au}^{-1}). After accounting for ECSA and Au loading, the ORR activity trend of Au_1NC-rGO < Au_9NC-rGO < Au_{101}NC-rGO is unchanged. Figure S3 presents the effect of Au mass loading (5%, 10%, and 20%) on the ORR activity of Au_{101}NC-rGO. We find the lower mass loading (5%) is far more efficient.

To investigate the durability and stability of the AuNCs-rGO, repeated LSV scanning and chronoamperometry measurement were conducted in O_2-saturated 0.1 M KOH under continuous O_2 flow and compared with Pt/C. The stability test performed by the chronoamperometry measurement showed 10%, 20%, 20%, and 40% loss in current density after 22 h for Au_{101}NC-rGO, Au_9NC-rGO, Au_1NC-rGO, and Pt/C, respectively (Figure 3b). The durability test measured by repeated LSV scanning showed a loss of 22%, 22%, and 35% in the current density (at 0.8 V *vs.* RHE) after 24 h for Au_1NC-rGO, Au_9NC-rGO, and Pt/C, respectively (Figure 4). In startling contrast, Au_{101}NCs-rGO shows an increased current density of 21%. Overall, the AuNCs-rGO showed a much smaller decay in the current density compared to the Pt/C, indicating greater stability of the AuNCs-rGO than Pt/C under the ORR conditions investigated.

2.1.3. Methanol tolerance activity investigation of AuNCs-rGO

Figure 5 shows the LSV traces for Au_1NC-rGO, Au_9NC-rGO, Au_{101}NC-rGO, and Pt/C in O_2-saturated 0.1 M KOH solution within increasing methanol concentration (0, 0.5, 1, 2, 5 M). For Pt/C, the ORR response at 0.94 V *vs.* RHE disappears, and a characteristic methanol oxidation peak is clearly observed at 0.81 V *vs.* RHE. In contrast, the LSV curves of Au_1NC-rGO, Au_9NC-rGO, and Au_{101}NC-rGO are almost unchanged in the presence of methanol.

This difference is further highlighted in the CV curves, where the characteristic peaks for methanol oxidation are observed at 0.80 V *vs.* RHE for Pt/C while no noticeable change is observed for Au_1NC-rGO, Au_9NC-rGO, and Au_{101}NC-rGO under the same conditions (Figure S11 (a–d)). These results show that the AuNCs-rGO ORR activity remains unchanged in the presence of

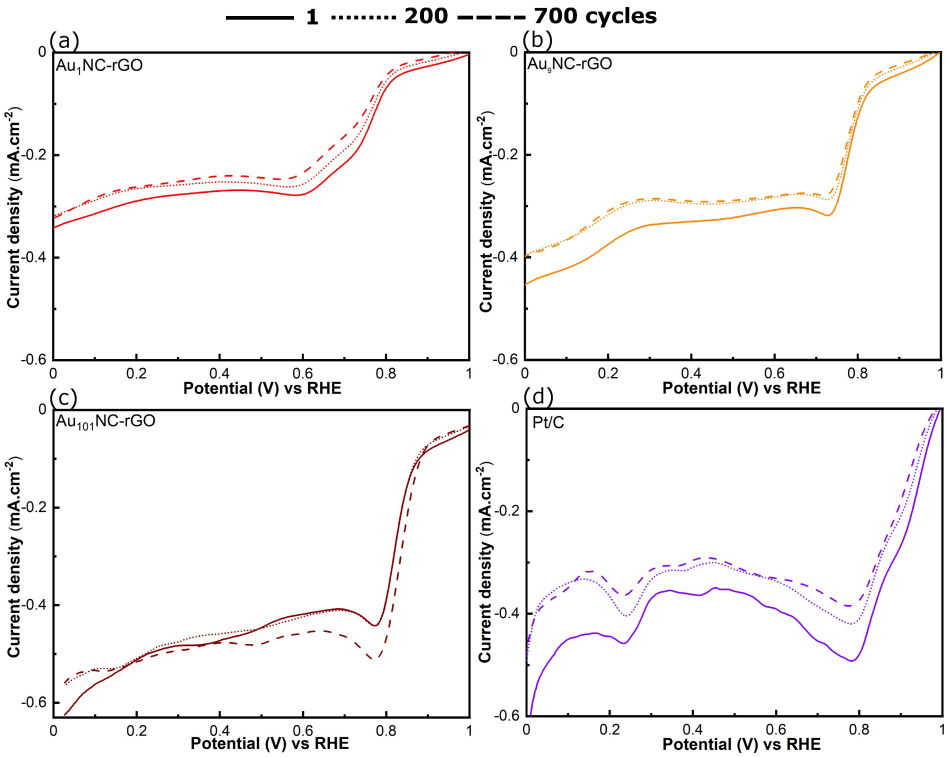

Figure 4. (a–d) Durability test of Au_1NC-rGO, Au_9NC-rGO, Au_{101}NC-rGO, and Pt/C by repeating the potential scan from +1.2 to 0 V (vs. RHE) at 10 mV s^{-1} in O_2-saturated 0.1 M KOH under continuous O_2 flow after 1, 200, and 700 scans (24 h).

methanol, even at the highest methanol concentration (5 M) for all AuNCs investigated.

2.2. Discussion

2.2.1. Oxygen Reduction Reaction

Table S1 presents the detailed experimental parameters of reported ORR studies using the AuNCs along with the current study. Figure 6 graphically displays the onset potential and current density at 0.8 V *vs.* RHE from the reported literature (since the Au mass loading within each work is different, the current density at 0.8 V *vs.* RHE per Au mass loading (mA mg_{Au}^{-1}) was chosen).

There have been a few studies on ORR using sub-2 nm AuNCs using different linear (*e.g.* p-MBA,[23] $SC_{12}H_{25}$,[12] PET,[15] and SC_2H_4Ph[16]) and bulky (*e.g.* PPh_3,[11] S-tBu,[17] and SR[18]) ligands. As discussed in the introduction, the contribution of different factors such as Au cluster size (number of Au atoms) and ligand type/density can play a key role in the ORR activity. PPh_3 is a bulky ligand for which previous experiments have shown that ligand density is the major factor affecting ORR performance.[17,18] We observe a direct correlation of lower ligand density resulting in greater ORR activity with the trend of $Au_{101} > Au_9 > Au_1$. The ligand density impacts the analyte diffusion/adsorption at AuNCs.[44] The higher ligand density in Au_1 and Au_9 results in a larger analyte diffusion/adsorption barrier and lower ORR activity than Au_{101}. We have previously reported greater HER performance for Au_{101}NC-rGO compared to Au_1NC-rGO and Au_9NC-rGO.[42]

In order to compare our reported data to literature value, we must consider some limitations in doing so. Electrocatalysis is highly dependent on the geometry of the electrode and the loading of the catalyst.[45] Unfortunately, these aspects are rarely consistent between publications, so direct comparison of values should be undertaken cautiously. In general, Table S1 and Figure 6 reveal that the onset potential is greater in alkaline media than acidic[15] and natural media.[22] In addition, low Au loading (less than 5 μg cm^{-2}) and size of AuNCs between 1.4–1.8 nm supported on rGO results in a higher current density (mA mg^{-1}) at 0.8 V *vs.* RHE.[13,20] Moreover, by increasing the size, the onset potential decreases for both unsupported AuNCs with linear ligands[11,15,16] and supported size specific AuNCs with removed ligands.[16] While the opposite trend was observed for supported size specific AuNCs with bulky ligands.[17,18] Here, Au_{101}NC-rGO exhibits the highest values for both parameters, onset potential and current density at 0.8 V *vs.* RHE (mA mg^{-1}) compared to the previously reported values for ORR.

The size-dependent stability was observed with the trend of Au_{101}NC-rGO > Au_9NC-rGO ~ Au_1NC-rGO. In our previous work, we showed that decreasing the AuNCs size results in easy agglomeration due to weak AuNCs-support interaction and high surface energy evidenced by XPS.[42] Therefore, Au_1 and Au_9 are readily agglomerated during chronoamperometry measurements. This result suggests high stability and agglom-

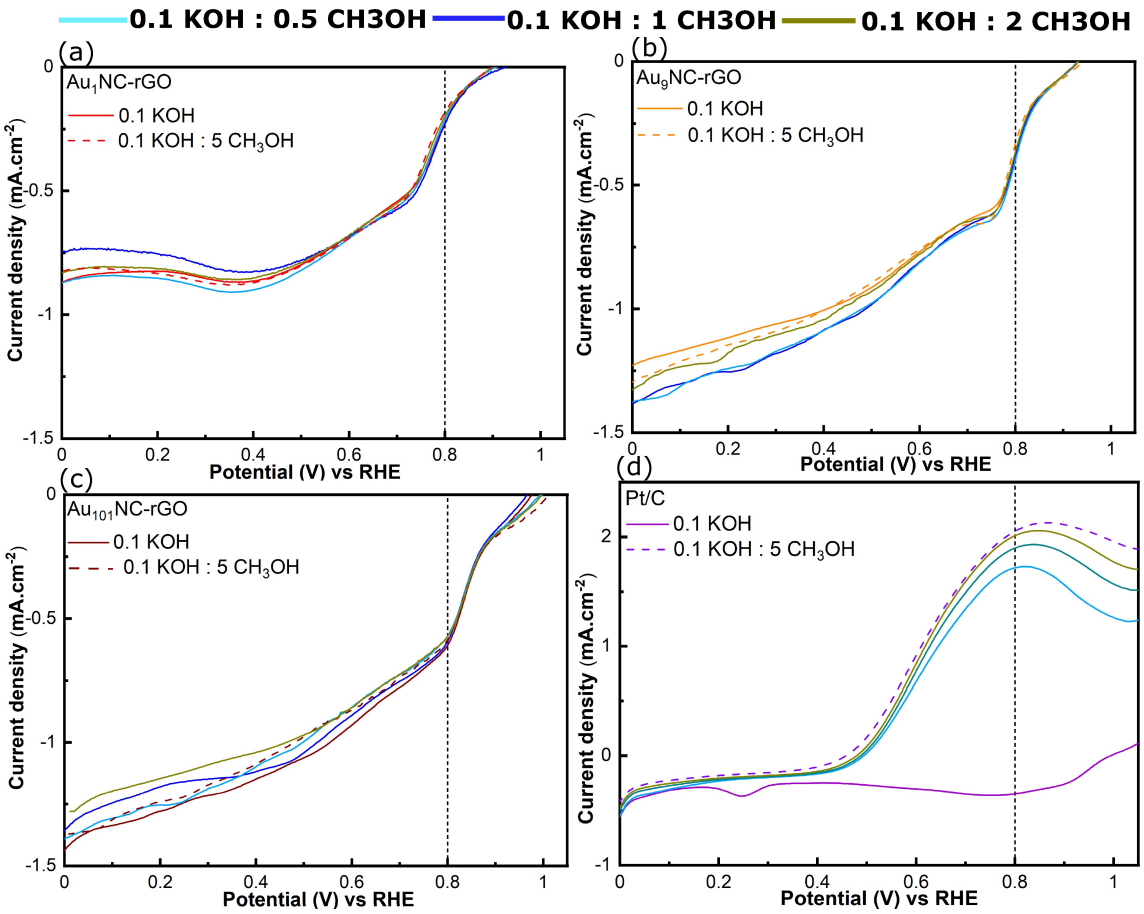

Figure 5. (a–d) ORR polarization curves in O_2-saturated 0.1 M KOH containing different concentration of CH_3OH (0, 0.5, 1, 2, 5 M) for Au_1NC-rGO, Au_9NC-rGO, Au_{101}NC-rGO, and Pt/C. All data was collected at a scan rate of 10 mV s^{-1}.

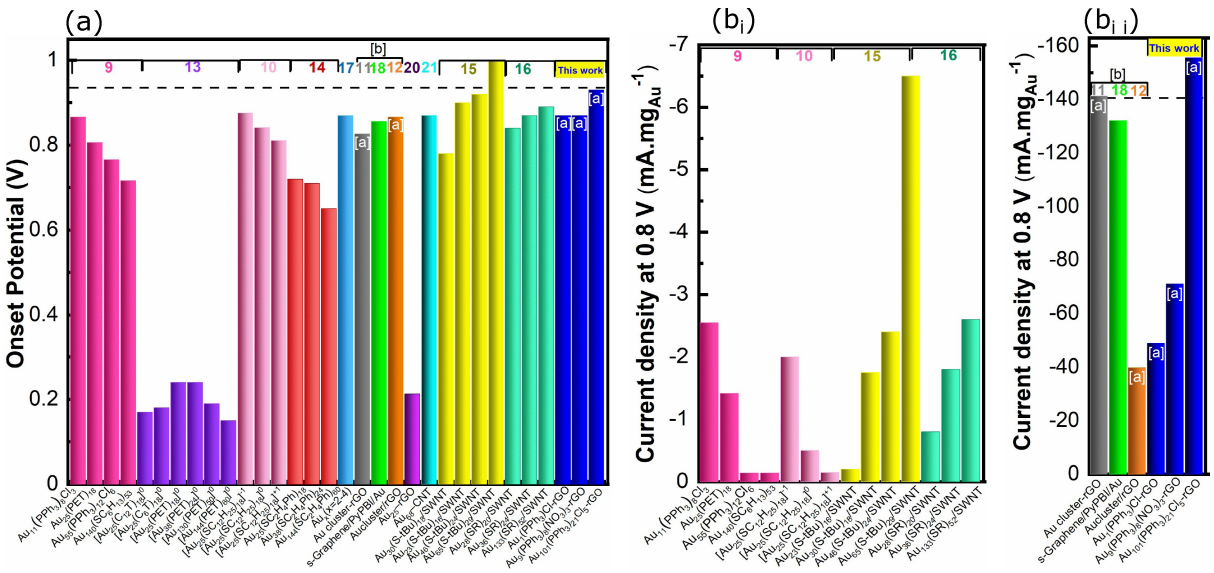

Figure 6. (a) Comparison of the onset potential and (b) the current density at 0.8 V (vs. RHE) per the actual Au mass loading (mA mg_{Au}^{-1}) of electrocatalysts with Au cluster size < 2 nm in Table S1 (b_i and b_{ii} have different Y-axis ranges for easier comparison). SWNT: single walled carbon nanotube, PPh_3: triphenylphosphine, $C_{12}T$ = 1-dodecanethiol, C_6T = 1-hexanethiol, PET = 2-phenylethanethiol, p-MBA = p-mercaptobenzoic acid, SC_6H_{13} = 1-hexanethiolate, $SC_{12}H_{25}$ = 1-dodecanethiol, SC_2H_4Ph = phenylethylthiolate, SR = 4-tert-butylbenzenethiol, S-tBu = tert-butylthiol. [a]: Methanol tolerance investigated. [b] no ligands used in AuNCs synthesis.

eration resistance of Au_{101}NC-rGO caused by the larger size and stronger metal-support interaction over Au_1NC-rGO and Au_9NC-rGO.

Table S1 reveals that the stability and durability of the electrocatalysts during ORR has received limited attention with only three studies. AuNC-rGO (2.4 ± 0.7 nm with removed polyvinyl pyrrolidone ligands, not size specific),[21] Au_{102}(p-MBA)$_{44}$-C (2.59 ± 0.70 nm with removed p-MBA ligands),[24] and Au cluster/rGO (1.8 ± 0.2 nm with no ligands, not size specific)[14] exhibited 6% (5 h), 25% (8 h), and 16% (11 h) loss in current density, respectively. In comparison Au_{101}NC-rGO in this study (1.44 ± 0.41 nm with PPh_3 ligands) experienced loss of 6%, 8%, and 10% in current density after 5, 8, and 11 h, respectively.

In general, these data reveal that the stability of AuNCs decreased for samples containing particles with size greater than 2.4 nm and less than 1 nm during chronoamperometry measurements. In addition, the similar stability (6% after 5 h) between Au_{101}NC-rGO and AuNC-rGO with different sizes suggests that the stability of AuNCs is influenced not only by the size but also by the ligand. The presence of ligands prevents easy agglomeration of particles during chronoamperometry measurements resulting in the stability improvement of AuNCs over AuNCs with removed or no ligands.

2.2.2. Methanol tolerance

There are very limited investigations relating to the methanol tolerance for AuNCs, with 2 studies showing that AuNCs are methanol tolerant.[13,14] In the case of methanol cross over: O_2, H_2O, and CH_3OH are in strong competition for the adsorption sites at the cathode. The rate of ORR and MOR depends on the degree of O_2 and methanol absorptions with the active sites of the AuNCs.

Figure 5 highlights the excellent size-independent methanol tolerance of the AuNCs-rGO even at the highest methanol concentration (5 M) compared to the Pt/C (the highest reported methanol concentration for Au cluster in literature is 3 M).[13,14] As discussed in the introduction, the inherent large onset potential of Au for methanol oxidation prevents the easy formation of CO from methanol which restricts MOR (see indirect MOR mechanism in Figure 1).[10,46] In contrast, Pt oxidizes methanol easily to CO owing to its lower ΔG_{CO} but has difficulty in oxidizing CO to CO_2 due to its poor ability to activate water (higher ΔG_{OH}: Gibbs free energy for water activation to hydroxyl), thus poisoning its catalytic activity toward ORR.

The size-independent methanol tolerance of AuNCs-rGO suggests that the presence of the PPh_3 ligands could also increase the methanol tolerance. It has been reported that the presence of ligands can have beneficial effects to improve the catalytic activity and/or selectivity caused by steric, electronic, and solubility effects.[47] The steric effect of ligand results in boosting the selectivity of a particular reaction on the surface of the catalyst. The size of the ligand can restrict the access of large molecules like methanol and have no effect on the accessibility of small molecules such as O_2. The electronic densities of metals can be tuned by the ligands, which promote the adsorption and activation of the molecules on the surface of metals, enhancing the catalytic activity. Ligand also can generate a hydrophobic surface on the metal, which can affect the solubility of the molecules, specifically gasses like O_2 and enhance ORR. Lu *et al.* showed experimentally and theoretically that PPh_3 could have a significant effect on ORR and methanol tolerance of Pt caused by the combined electronic and steric effects of PPh_3.[48] PPh_3 as an electron-donating ligand increases the negative charge on Pt surface. The negative steric effect of PPh_3 on Pt, facilitates O_2 absorption/activation and weakens methanol absorption, which results in MOR activity reduction and ORR enhancement compared to Pt without ligands.

2.2.3. Consequences for direct methanol fuel cells

As discussed in the introduction, bulk Au has a high overpotential for both ORR and MOR. The data in Table S1 and Figure 6, along with our results, demonstrate that the ORR and MOR activity and selectivity of AuNCs at the cathode is dependent on the oxygen and methanol adsorption ability on the Au surface, influenced by both size and ligand. Downsizing the bulk Au to less than 2 nm in size improves the activity towards ORR without affecting MOR. However, lower ligand density as a second factor also comes into effect on catalytic activity and selectivity of AuNCs with larger particle sizes. Au_{101} with the larger size and lower ligand density provides the best overall structure for adsorption/activation of O_2 compared to Au_1 and Au_9. Future work is required to investigate and synthesise the best structure of PPh_3-ligated AuNCs with the optimal size and composition to achieve high ORR activity, closer to commercial Pt/C or other methanol tolerant ORR catalysts using the presented methodology.

3. Conclusions

Size-specific PPh_3-ligated AuNCs supported on rGO were investigated as methanol tolerant ORR electrocatalysts. Our AuNCs-rGO electrocatalysts exhibited size-independent methanol tolerance and size-dependent ORR activity. ORR activity increased with cluster size. The highest ORR activity for Au_{101}NC-rGO results from a range of factors, including size, ligand density, and electronic effects. Irrespective of the size of AuNCs, the inherent large onset potential of Au toward methanol oxidation, along with the presence of PPh_3 ligands, could be the reasons for methanol tolerance of AuNCs.

In comparison with Pt/C, the three different size AuNCs-rGO exhibited lower ORR activity but greater stability and durability over 24 h, along with excellent methanol tolerance. In addition, Au_{101}NC-rGO exhibited enhanced durability after 24 h, while Au_1NC-rGO, Au_9NC-rGO, and Pt/C showed reduced activity.

This work creates an opportunity for further research and development of high-performance graphene-triphenylphosphine ligated AuNCs-based as cathode electrocatalysts for DMFCs.

Experimental Section

Working electrode construction

All catalyst suspensions were prepared following our previously reported procedure (complete details are in SI).[25] 45.0 μg cm^{-2} of the as-prepared AuNCs-rGO (Au_1NC-rGO, Au_9NC-rGO, and Au_{101}NC-rGO, all 5% wt Au), 42.4 μg cm^{-2} of rGO, and 11.2 μg cm^{-2} (containing 2.25 μg cm^{-2} Pt) 20% commercial Pt/C (all dispersed in methanol) were cast onto a polished GCE. Nafion was then dropped onto the GCE (0.7 μL of 5 wt % Nafion solution). The as-obtained AuNCs (Au_1, Au_9, and Au_{101}) were dispersed in methanol (0.5 mg mL^{-1}, non-ligated Au mass) and 2.25 μg cm^{-2} of each AuNCs dispersion was cast onto polished GCE followed by casting 0.3 μL of 5 wt % Nafion solution. All modified electrodes were dried at room temperature (RT) for 2 h before electrochemical measurements. The polished and modified GCE was dried by a gentle N_2 flow for 1 min before the experiments.

Electrochemical measurements

All electrochemical measurements were accomplished on a potentiostat/galvanostat (Autolab PGSTAT204) in a three-electrode electrochemical set up at a scan rate of 10.0 mV s^{-1} in a 0.1 M KOH aqueous solution (pH = 13) at RT. The as-prepared catalyst coated GCE with a geometric surface area of 0.071 cm^2 (3 mm diameter) was used as the working electrode. An Ag/AgCl (3 M KCl) and Pt wire were used as reference electrode and counter electrode, respectively. The bare GCE was subjected to mechanical polishing with 0.05 μm alumina powder on a polishing microcloth prior to casting. N_2 or O_2 was purged into the solutions for 30 min prior and throughout all experiments to achieve an O_2-free or O_2-saturated state. To investigate the ORR activity and methanol tolerance, CV and LSV were applied within the potential range of −1.0 and +0.2 V *vs.* Ag/AgCl. For the methanol tolerance, CV and LSV of each AuNCs-rGO and Pt/C were performed in the presence of a given concentration of methanol (0, 0.5, 1, 2 and 5 M) in the O_2-saturated electrolyte. Note that all LSV curves are reported after 20 scans (i.e. the 20th scan). All the obtained potentials were referenced toward the RHE (Reversible Hydrogen Electrode) following:

$$E_{RHE} = E_{Ag/AgCl} + 0.059pH + E^{\circ}_{Ag/AgCl}\ (0.210^{*}\ V).$$

*The potential of an Ag/AgCl reference electrode with respect to the RHE using 3 M KCl at 25 °C.[49]

Durability and Stability measurements

The durability for AuNCs-rGO and Pt/C was performed by repeated LSV scans from +0.2 to −1.0 V (*vs.* Ag/AgCl) for 24 h (700 scans). The stability of AuNCs-rGO and Pt/C toward ORR was examined by chronoamperometric measurements at the $E_{1/2}$ for 22 h. Both stability (constant potential) and durability (repeated scanning) were performed in the O_2-saturated 0.1 M KOH solution under continuous O_2 flow at a sweep rate of 10 mV s^{-1}.

Double-layer capacitance and electrochemical active surface area

C_{dl} of the catalytic surface and ECSA of AuNCs-rGO were evaluated by CV at non-Faradaic potential ranging from 0 to 0.1 V (*vs.* Ag/AgCl) at different scan rates (5, 10, 20, 40, 50, 80, 100 mV s^{-1}) in a N_2-saturated 0.1 M KOH solution. C_{dl} was evaluated from the slope of linear regression of the ΔJ $(J_a - J_c)/2$ at 0.05 V (*vs.* Ag/AgCl) against the scan rate. J_a and J_c are the current density of anode and cathode at 0.05 V (*vs.* Ag/AgCl).

Onset and $E_{1/2}$ determination

Figure S5 presents the methods to calculate the key parameters, onset potential and $E_{1/2}$, extracted from LSV curves. The onset potential was determined from the starting potential where oxygen reduction begins by faradaic current amplification using a linear fit. $E_{1/2}$ is the potential at which the current is one half of the oxygen reduction peak which was calculated from the maximum point of the 1st derivative of LSV.

Acknowledgements

This work was supported by funding from The Australian Solar Thermal Research Initiative (ASTRI) program, which, is supported by the Australian Government, through the Australian Renewable Energy Agency (ARENA). HM wishes to acknowledge the University of Adelaide for the awarding of a postgraduate scholarship. The authors acknowledge the facilities of Adelaide Microscopy (University of Adelaide). CJS acknowledges funding support from The Australian Research Council (ARC) for a Future Fellowship (FT190100854). Open access publishing facilitated by The University of Adelaide, as part of the Wiley - The University of Adelaide agreement via the Council of Australian University Librarians.

Conflict of Interest

The authors declare no conflict of interest.

Data Availability Statement

The data that support the findings of this study are available from the corresponding author upon reasonable request.

Keywords: direct methanol fuel cell · electrocatalysis · gold clusters · methanol tolerance oxygen reduction reaction · reduced graphene oxide

[1] G. Thomas, in *US DOE Hydrogen Program 2000 Annual Review*, May 9–11, **2000**, San Ramon, California
[2] K. T. Møller, T. R. Jensen, E. Akiba, H.-w. Li, *Prog. Nat. Sci.* **2017**, *27*, 34–40.
[3] A. Poluzzi, G. Guandalini, S. Guffanti, M. Martinelli, S. Moioli, P. Huttenhuis, G. Rexwinkel, J. Palonen, E. Martelli, G. Groppi, M. C. Romano, *Front. Energy Res.* **2022**, *9*.
[4] X. Zhang, S.-X. Guo, K. A. Gandionco, A. M. Bond, J. Zhang, *Mater. Today* **2020**, *7*, 100074.
[5] K. Scott, L. Xing, in *Advances in Chemical Engineering, Vol. 41* (Ed.: K. Sundmacher), Academic Press, **2012**, pp. 145–196.
[6] M. Asteazaran, S. Bengio, W. E. Triaca, A. C. Luna, *J. Appl. Electrochem.* **2014**, *44*, 1271–1278.
[7] J. N. Tiwari, R. N. Tiwari, G. Singh, K. S. Kim, *Nano Energy* **2013**, *2*, 553–578.
[8] S. Q. Song, W. J. Zhou, W. Z. Li, G. Sun, Q. Xin, S. Kontou, P. Tsiakaras, *Ionics* **2004**, *10*, 458–462.
[9] J. K. Nørskov, J. Rossmeisl, A. Logadottir, L. Lindqvist, J. R. Kitchin, T. Bligaard, H. Jónsson, *J. Phys. Chem. B* **2004**, *108*, 17886–17892.

[10] P. Ferrin, A. U. Nilekar, J. Greeley, M. Mavrikakis, J. Rossmeisl, *Surf. Sci.* **2008**, *602*, 3424–3431.
[11] W. Chen, S. Chen, *Angew. Chem. Int. Ed.* **2009**, *48*, 4386–4389; *Angew. Chem.* **2009**, *121*, 4450–4453.
[12] Y. Lu, Y. Jiang, X. Gao, W. Chen, *Chem. Commun.* **2014**, *50*, 8464–8467.
[13] S. Xu, P. Wu, *J. Mater. Chem. A* **2014**, *2*, 13682–13690.
[14] H. Yin, H. Tang, D. Wang, Y. Gao, Z. Tang, *ACS Nano* **2012**, *6*, 8288–8297.
[15] B. Kumar, T. Kawawaki, N. Shimizu, Y. Imai, D. Suzuki, S. Hossain, L. V. Nair, Y. Negishi, *Nanoscale* **2020**, *12*, 9969–9979.
[16] L. Wang, Z. Tang, W. Yan, H. Yang, Q. Wang, S. Chen, *ACS Appl. Mater. Interfaces* **2016**, *8*, 20635–20641.
[17] T. C. Jones, L. Sumner, G. Ramakrishna, M. b. Hatshan, A. Abuhagr, S. Chakraborty, A. Dass, *J. Phys. Chem. C* **2018**, *122*, 17726–17737.
[18] L. Sumner, N. A. Sakthivel, H. Schrock, K. Artyushkova, A. Dass, S. Chakraborty, *J. Phys. Chem. C* **2018**, *122*, 24809–24817.
[19] T. Huang, Z.-h. Sun, G.-q. Pan, *Chin. J. Chem. Phys.* **2018**, *31*, 66.
[20] T. Fujigaya, C. Kim, Y. Hamasaki, N. Nakashima, *Sci. Rep.* **2016**, *6*, 21314.
[21] C. Wang, N. Li, Q. Wang, Z. Tang, *Nanoscale Res. Lett.* **2016**, *11*, 336.
[22] K. Kwak, U. P. Azad, W. Choi, K. Pyo, M. Jang, D. Lee, *ChemElectroChem* **2016**, *3*, 1253–1260.
[23] C. Zúñiga Loyola, A. G. Caro, J. Govan, G. Abarca, W. Orellana, F. Tasca, *Mater. Chem. Front.* **2021**, *5*, 7529–7539.
[24] Q. Wang, L. Wang, Z. Tang, F. Wang, W. Yan, H. Yang, W. Zhou, L. Li, X. Kang, S. Chen, *Nanoscale* **2016**, *8*, 6629–6635.
[25] H. Mousavi, Y. Yin, L. Howard-Fabretto, S. K. Sharma, V. Golovko, G. G. Andersson, C. J. Shearer, G. F. Metha, *Nanoscale Adv.* **2021**, *3*, 1422–1430.
[26] G. Li, R. Jin, *JACS* **2014**, *136*, 11347–11354.
[27] a) O. Lopez-Acevedo, K. A. Kacprzak, J. Akola, H. Häkkinen, *Nat. Chem.* **2010**, *2*, 329–334; b) W. Liu, Y. F. Zhu, Q. Jiang, *J. Phys. Chem. C* **2010**, *114*, 21094–21099.
[28] Y. Pei, N. Shao, Y. Gao, X. C. Zeng, *ACS Nano* **2010**, *4*, 2009–2020.
[29] M. Turner, V. B. Golovko, O. P. Vaughan, P. Abdulkin, A. Berenguer-Murcia, M. S. Tikhov, B. F. Johnson, R. M. Lambert, *Nature* **2008**, *454*, 981–983.
[30] J. Kilmartin, R. Sarip, R. Grau-Crespo, D. Di Tommaso, G. Hogarth, C. Prestipino, G. Sankar, *ACS Catal.* **2012**, *2*, 957–963.
[31] R. H. Adnan, G. G. Andersson, M. I. Polson, G. F. Metha, V. B. Golovko, *Catal. Sci. Technol.* **2015**, *5*, 1323–1333.
[32] Y. Du, H. Sheng, D. Astruc, M. Zhu, *Chem. Rev.* **2020**, *120*, 526–622.
[33] T. Kawawaki, Y. Negishi, *Nanomaterials* **2020**, *10*, 238.
[34] M. L. Ganadu, F. Demartin, A. Panzanelli, E. Zangrando, M. Peana, S. Medici, M. A. Zoroddu, *Molecules* **2021**, *26*, 5014.
[35] J. A. van Bokhoven, J. T. Miller, *J. Phys. Chem. C* **2007**, *111*, 9245–9249.
[36] N. S. Phala, E. van Steen, *Gold Bull.* **2007**, *40*, 150–153.
[37] M. Rambukwella, N. A. Sakthivel, J. H. Delcamp, L. Sementa, A. Fortunelli, A. Dass, *Front. Chem.* **2018**, *6*, 330.
[38] M. Liu, R. Zhang, W. Chen, *Chem. Rev.* **2014**, *114*, 5117–5160.
[39] M. Hu, Z. Yao, X. Wang, *Ind. Eng. Chem. Res.* **2017**, *56*, 3477–3502.
[40] S. Stolbov, M. A. Ortigoza, *J. Chem. Phys.* **2015**, *142*, 154703.
[41] X. Chen, S. Sun, F. Li, X. Wang, D. Xia, *Molecules* **2013**, *18*, 3279–3291.
[42] H. Mousavi, Y. Yin, S. K. Sharma, C. T. Gibson, V. Golovko, G. G. Andersson, C. J. Shearer, G. F. Metha, *J. Phys. Chem. C* **2022**, *126*, 246–260.
[43] P. Rheinlander, S. Henning, J. Herranz, H. A. Gasteiger, *ECS Trans.* **2013**, *50*, 2163–2174.
[44] S. L. Young, J. E. Kellon, J. E. Hutchison, *JACS* **2016**, *138*, 13975–13984.
[45] S. Anantharaj, S. Kundu, *ACS Energy Lett.* **2019**, *4*, 1260–1264.
[46] G. A. Tritsaris, J. Rossmeisl, *J. Phys. Chem. C* **2012**, *116*, 11980–11986.
[47] L. Lu, S. Zou, B. Fang, *ACS Catal.* **2021**, *11*, 6020–6058.
[48] L. Lu, Z. Wang, S. Zou, Y. Zhou, W. Hong, R. Li, L. Xiao, J. Liu, X.-Q. Gong, J. Fan, *J. Mater. Chem. A* **2018**, *6*, 18884–18890.
[49] S. Hernández, C. Ottone, S. Varetti, M. Fontana, D. Pugliese, G. Saracco, B. Bonelli, M. Armandi, *Materials* **2016**, *9*, 296.

Manuscript received: March 17, 2022
Revised manuscript received: May 2, 2022
Accepted manuscript online: May 9, 2022
Version of record online: June 7, 2022